October 5, 2010 (revised)

Spherical harmonic-based random fields based on real particle 3D data: Improved numerical algorithm and quantitative comparison to real particles

X. Liu[a] and E.J. Garboczi
National Institute of Standards and Technology
Materials and Construction Research Division
Gaithersburg, Maryland 20899-8615 USA

M. Grigoriu
Cornell University
Department of Civil and Environmental Engineering
Ithaca, New York USA 14853

Y. Lu
Virginia Tech
Department of Civil Engineering
Blacksburg, Virginia USA 24061

Sinan T. Erdoğan
Middle East Technical University
Department of Civil Engineering
Ankara, Turkey 06531

Abstract

The shape of particles often plays an important role in how they are used and in the properties of composite systems in which they are incorporated. When building models of systems that include real particles, it is often of interest to generate new, virtual particles whose 3D shape statistics are based on the 3D shape statistics of a collection of real particles. A previous paper showed mathematically how this can be carried out, but only had a small set of real particle shape data to use and only made a limited amount of qualitative comparisons to the real particle data. The present paper shows how the numerical method used to create virtual particles has been improved and immensely accelerated, allowing the use of large particle data sets. Making use of several large particle shape data sets, the paper confirms that the algorithm creates particles whose statistical shape properties closely match the real particles from which they were generated. Another question that can now be addressed with these larger particle datasets is: how many real particles are enough to be representative of the particle class from which they were drawn? The types of particles analyzed include two size ranges of crushed granite-hornblende rocks, silica sand, calcium carbonate powder, and ground granulated blast furnace slag.

Key words: shape; 3D; spherical harmonics; virtual particles

---

[a] Permanent address: College of Geo-Resources and Information, China University of Petroleum (East China), Dongying, Shandong Province, China

1. Introduction:

Many materials used in current technology are classified as particles - discrete clumps of solid matter that range in size from a few nanometers (molecules, quantum dots) to meters or more (boulders). Many materials are used in powder form, where the term 'powder' usually means individual particles that are well less than a millimeter in dimension. Sands are often used in construction, and their particle size is usually on the order of several millimeters. Gravels, whether of natural origin or crushed from larger rocks, have sizes ranging from a few millimeters on up to perhaps 20 mm. Whatever their size, the way particulate materials are used and their properties either as individual particles or as a packing of particles or as inclusions in a matrix [1,2] often depend upon their 3D shape.

There have been many attempts to quantify particle shape [3]. In recent years, a method of acquiring a 3D image using X-ray tomography (X-ray CT), followed by spherical harmonic (SH) analysis, has been used successfully for star-shaped particles. A star-shaped object requires that all line segments that connect the center of mass to any point inside the body (or on its surface) lie entirely within the body. This method completely analyzes particle shape, within the resolution limits of the original X-ray CT images, and results in an accurate, analytic formula for the length from the center of mass of the particle to any point on its surface, $r(\theta,\phi)$, as a function of the two spherical polar angles (θ,ϕ) [4-7]. Any property that can be defined by analysis of this function, including volume and surface integrals, can be calculated. This technique has been applied to analyze the shape of different particles and relate them to other properties and other measurement techniques [8-10]. Laser surface scanning can also give the required starting images [11], as well as focused ion beam tomography [12].

In building models using real 3D particles, one could simply use the real particles whose shape has been characterized by SH analysis. However, for more generality one would like to be able to generate arbitrary numbers of particles whose shape and size statistics closely match a target population of real particles. An attempt to do this was carried out in a recent paper [13]. The mathematical apparatus was developed and used, based on a population of 128 real particles, to generate virtual particles, but only a limited amount of qualitative comparison was made to the real particles. This present paper, which is a sequel to Ref. [13], greatly improves the numerical method used to create virtual particles, so that much larger sets of real particles can be used for a basis for virtual particle generation. Making use of several large particle shape data sets, the paper confirms that the algorithm creates particles whose statistical shape properties closely match the real particles from which they were generated. Another question that can now be addressed with these larger particle datasets is: how many real particles are enough to be representative of the particle class from which they were drawn? Several real, 3D particle shape data sets of different mineralogy and origins are used to generate virtual particles, compare to the real particles using various quantitative shape parameters, and address these issues.

2. Experiments, Materials and Data

The X-ray CT results presented in this paper were collected on two instruments: (1) beamline X2B, at the National Synchrotron Light Source (NSLS), Brookhaven National Laboratory, and (2) on a benchtop instrument located at the National Institute of Standards and Technology (NIST). In X-ray CT, X-rays penetrate a 3D sample at many different angles and the absorption is measured. A computer-based reconstruction technique then makes gray level

images, where each image is a slice of the sample and the contrast in gray levels is caused by the different X-ray absorption properties of the materials in the sample.

Voxel sizes ranging from about 20 μm down to slightly less than 1 μm were used. The particles were embedded in epoxy in a cylindrical polymer mold and then scanned. The reconstructed image slices were stacked into 3D microstructures consisting of gray scale images of particles embedded in a matrix. A suite of image analysis and error correction software was used to create a binary image of white, separated particles in a black matrix. Custom software was used to extract each individual particle's set of voxels in 3D [6].

The spherical harmonic mathematical analysis relies on eq. (1), which states that any sufficiently smooth function $r(\theta,\phi)$, where θ and ϕ are the azimuthal and polar angles of 3D spherical coordinates, can be written as a series of spherical harmonic functions, where the Y_{nm} are the complex spherical harmonic (SH) functions and the A_{nm} are complex coefficients [14]:

$$r(\theta,\phi) = \sum_{n=0}^{N} \sum_{m=-n}^{n} A_{nm} Y_{nm}(\theta,\phi) \qquad (1)$$

Strictly speaking, the series in eq. (1) becomes exact only as $N \to \infty$. However, like 2-D Fourier series, a finite value of N is usually found to give an adequate approximation of a given function, within some specified uncertainty limit as defined by the integrated Gaussian curvature [4]. A thorough uncertainty analysis of this combined X-ray CT/SH method has been carried out previously [4]. Using a numerically determined $r(\theta,\phi)$ function from a 3D voxel image of a single particle, one can accurately determine the first N = 20 or so coefficients in eq. (1), which are usually enough to satisfactorily represent the particle. In the cases studied in this paper, the average value of N used for a particle class ranged from 20 to 24 across different kinds of particles.

The SH coefficients can be used to compute any surface or volume integral over a particle, since eq. (1) gives an analytic function for the particle's shape. Therefore, any shape parameter can be computed. Several used in this paper include the volume equivalent spherical diameter (VESD), which is the diameter of a sphere with volume equal to the volume of a given particle. The principal moments of inertia are used, defined by diagonalizing the moment of inertial tensor [4]. Their ratios can also be used as a kind of aspect ratio [15]. The mean curvature and standard deviation of the mean curvature is also used, both at a surface point and average over the particle surface (more on these parameters later in the paper) [4].

There are also shape parameters that are not defined by a surface or volume integral. Three useful parameters are the length (L), the width (W), and the thickness (T) [5]. Any one of these three can also serve as a particle dimension, as the VESD can, although a randomly shaped particle cannot be completely characterized by a single dimension [7]. The length (L) is defined as the largest straight-line surface point-to-surface point distance on the particle. The width (W) is defined similarly, except that it must be perpendicular to the length. The thickness (T) is also defined similarly, except that it must be perpendicular to both the length and the width. The dimensions L, W, and T define some kind of equivalent rectangular parallelepiped for the irregular particle, with $L \geq W \geq T$.

A variety of particles were used in this study. Table 1 lists the sources and kinds of particles used. All were commercial inorganic minerals. Images of all the particles were extracted and their associated SH coefficients stored in a database. Column 5 of Table 1 lists

how many particles were obtained for each particle type. The average values of the L/T ratio (length to thickness) and W/T ratio (width to thickness) are recorded in the last two columns. These serve as aspect ratios for the particles, but do not address questions of angularity or roughness. The images of the materials with a smaller number of particles were obtained on the Brookhaven beam line, where there was less opportunity to obtain multiple image sets. Images of the Wilson particles were obtained on a local X-ray CT, where more scan time was available for obtaining a larger number of particles images. Column 4 of Table 1 gives the upper size limit of each particle type in terms of the VESD value. This quantity can easily be computed for each particle analyzed.

3. Theory and Numerical Techniques

The mathematical details of the virtual particle generation algorithm were described in Ref. [13]. This paper follows Model 2 in [13]. Briefly, Model 2 can be viewed as a version of eq. (1) whose complex coefficients $\{A_{nm} = a_{nm} + i\, b_{nm}\}$ are random variables rather than deterministic constants. The first coefficient $A_{00}=a_{00}$ is real-valued and defines the particle size in the sense that most of its volume is within the equivalent sphere with radius (aside from a constant [4]) equal to a_{00}. The distribution of the values of a_{00} are fit by a gamma distribution, and then the series of coefficients for each real particle are normalized by the value of a_{00} for each series. The series of coefficients A_{nm} are scaled by a_{00} so that they correspond to particles of similar size. For computational convenience, the complex-valued variables A_{nm} are replaced by their real and imaginary parts, a_{nm} and b_{nm}. The model includes approximately the first n = 20 terms of the infinite series in eq.(1). In Ref. [13], the statistics of a_{nm} and b_{nm} were calculated for a data set consisting of 128 particles and used to calibrate the distributions of new random variables a_{nm} and b_{nm}. These distributions defined the randomized version of eq. (1). Model 2 was then used to generate virtual particles that were statistically consistent with the 128 original particles, with the fitted distribution of a_{00} used to make the size distribution of the virtual particles follow that of the original real particles.

When applying this algorithm to new sets of particles, it became clear that the shape of the A_{00} distribution for real particles was somewhat arbitrary, and depended only on exactly what set of particles were chosen to go into the original X-ray CT samples, what fraction of these particles were actually scanned, what fraction of the particles made it through the reconstruction process, and of course what was the original size distribution. Clearly, the $a_{00} = A_{00}$ distribution of Wilson A particles in Fig. 1a would be difficult to fit with a gamma distribution, which drove the improvement of the virtual particle algorithm to allow for arbitrary A_{00} distributions, not just those that could be well-fit by a gamma distribution. To make the algorithm applicable to an arbitrary size distribution of real particles, the actual numerical distribution of the A_{00} coefficients, in a cumulative probability form, was used instead of trying to fit the kind of distribution shown in Fig. 1a. However, Fig. 1b shows the same kind of distribution but for a_{31} and b_{31}, which are much more symmetrical and more easily fit by a gamma or beta distribution; therefore, a fitting function for these variables was continued. The higher order coefficients reflect the actual shape of the particles, and are much less influenced by the actual size of the particles. There could be some small dependence of shape on size for these particles, but in the size range considered here, this would not have an influence [12,16].

The codes used in Ref. [13] were written in MATLAB*, which is a cross-platform scientific software that provides simple methods to validate complicated algorithms. However, the code written in MATLAB ran too slowly to allow more than a few hundred real particles to be practically considered. By rewriting the algorithm in Fortran 90, a large speed-up was obtained. This code was then parallelized, so that many (10 000 +) real particles could easily be considered. Using larger number of real particles should allow better estimation of the various real particle moments that are needed to generate the virtual particle coefficients. There are two time consuming parts in the Model 2 algorithm: (1) computing the H matrix (a collection of coefficients that defines the shape of a particle) from the coefficients of the real particles, and (2) converting the H matrix for virtual particles, once generated, back into the coefficients of the spherical harmonic expansion. The two procedures for each particle are independent so that the parallelization is straightforward, using the Message Passing Interface (MPI) in the Single Program Multiple Data (SPMD) mode, improving the speed of the codes tremendously. The run time for generating 10 000 virtual particles based on 15 829 real particles was about 20 minutes using 100 processors, while a smaller computation for about 3000 real particles took about three weeks using the serial MATLAB code.

4. Results

The results for the Wilson A particles are examined first. Figure 2 shows the contrast between the old (fitting the a_{00} distribution) and new (directly using the a_{00} distribution) virtual particle results for the 15 829 Wilson A particles using the old and the new methods. Note that both versions of the algorithm were parallelized. Figure 2a shows the cumulative probability distribution for the VESD parameter. The solid line is the real particle result, which serves as a baseline. The solid points corresponding to the new method fall very accurately on the real particle result, while the old method results lie significantly far away from the real particle result. There were 10 000 virtual particles generated for each method, from which the probability distribution was derived. Figure 2b shows similar results but for the maximum principal moment of inertia tensor for each particle. To generate this data, the moment of inertia tensor was calculated for each particle, and then diagonalized to find the principal moments. It is clear that the algorithm improvement described above allows for accurate reproduction of the real particles' statistical attributes, both shape and size.

Figure 3 shows two 3D VRML (Virtual Reality Modeling Language) images, one of a real particle and one of a virtual particle made based on the real particles. The virtual particle was made using the new method introduced in this paper. Comparing the two images visually does not prove anything quantitative about their similarity, of course, but one could say that perhaps the virtual particle image has more "protuberances" on it than does the real particle image.

* Certain commercial equipment and/or materials are identified in this report in order to adequately specify the experimental procedure. In no case does such identification imply recommendation or endorsement by the National Institute of Standards and Technology, nor does it imply that the equipment and/or materials used are necessarily the best available for the purpose.

A vital question when generating virtual particles is: did the initial real particle dataset contain enough particles so that it accurately represented the class of particles from which the dataset was drawn? That question can be approached indirectly by considering how the statistical properties of subsets of the original dataset change as the subset becomes larger and larger. The improved algorithm allows the examination of particle datasets large enough to make it worthwhile to consider subsets (in Ref. [13], the real particle dataset contained only 128 particles). If these statistical shape properties flow to a nearly constant value for subsets of a size well less than the total dataset, then one can be reasonable confident that enough real particles have been used so that the real particle dataset, and consequently the virtual particles generated from this dataset, accurately reflect the particular particle class.

Figure 4 shows the cumulative probability distribution for the VESD parameter for virtual Wilson A particles generated from differing numbers of randomly selected real particles: 100, 1000, 5000, and 15 829. The results for all 15 829 real particles are also displayed as a baseline. It is clear that the virtual particle results (10 000 virtual particles were generated for each case) come closer and closer to the 15 829 particle results as an increased number of real particles was used to generate the virtual particle results. Figure 5 shows similar results for the maximum principal moment of inertia.

Figure 6 shows the average value of the L and VESD parameters as a function of the number of Wilson A particles in the real particle subset. The lines show the data for real particles, obtained by averaging over only that size subset of real particles. The data points show the average over 10 000 virtual aggregates, generated from different size subsets of real particles as shown on the abscissa. For each size real particle subset used, the virtual particle results closely match the real particle result, for both L and VESD, thus lending support to the accuracy of the algorithm used. Other statistical shape parameters showed similar behavior. However, these average values definitely decrease with the size of the real particle subset used. They perhaps flow to a nearly constant value by about 10 000 particles, but it is not clear. It is possible that 15 829 Wilson A particles are not quite enough to match the particle class from which they are drawn.

The discussion now turns to results on four other particle datasets, chosen for different mineralogies and/or different size ranges. The first two particles to be considered are the C109 sand and the Wilson B particles. The C109 sand is a standard sand [17], used across the country for many different kinds of tests [18]. The ASTM C109 test uses this sand to make standard mortars (cement + sand + water) to test for the effect of cement on compressive strengths of mortar cubes. The Wilson B particles are a smaller, more finely ground version of the Wilson A particles. Figure 7 shows 3D VRML images of two C109 sand particles, one real and one virtual. Although this comparison is only qualitative, it also hints that like in Fig. 3, the virtual particles tend to have more “lobes” than do the real particles. This point will be discussed more fully later in the paper. Figure 8 shows a similar comparison for two Wilson B particles, one real, one virtual.

Figure 9 shows the cumulative probability distributions for the VESD and maximum principal moment of inertia parameters for the C109 sand and the Wilson B particles, for both real and virtual particles. Good agreement between real and virtual particle results is shown for both kinds of particles, for both parameters, although the agreement for the VESD parameter seems to be a little better than for the moment of inertia parameter, similar to the behavior seen for the Wilson A particles.

Figure 10 shows how the statistical shape parameters of the real particles, L and VESD, vary with the size of the real particle subset used. There are no equivalent virtual particle results based on these subsets, as there were for the Wilson A particles. By about 5000 particles, the Wilson B results seem to have gained a nearly constant value, arguing that the total size of the real particle dataset used, 22 556, was large enough to be representative of the Wilson B particle class. Figure 11 shows the equivalent data for the C109 sand. In this case, only about 500 of these particles were enough to have the average value of the L and VESD parameters become nearly constant. In considering Table 1, the C109 particles were more uni-axed than were the Wilson B particles, in the sense of having L/T and W/T averages closer to one, which would be the result for a perfect sphere or cube.

Figure 12 shows 3D VRML images of two slag particles, one real and one virtual and Fig. 13 shows the same but for two calcium carbonate (CC) particles, one real, one virtual. Although this comparison is only qualitative, both figures hint, as did earlier figures, that the virtual particles tend to have more "lobes" than do the real particles. The cumulative probability distributions for the VESD and maximum principal moment of inertia parameters for the real and virtual slag and calcium carbonate particles are displayed in Fig. 14. Good agreement between real and virtual particle results is shown for both kinds of particles, for both parameters, although the agreement for the VESD parameter seems to be a little better than for the moment of inertia parameter. Again, there results are similar to those found earlier for the other particles.

Figure 15 shows how the statistical shape parameters of the real particles, L and VESD, vary with the size of the real particle subset used for the CC and slag particles. There are no equivalent virtual particle results based on these subsets, as there were for the Wilson A particles. By about 1000 particles, the average L and VESD parameters for both kinds of particles seem to have gained a nearly constant value, arguing that the total size of the real CC particle dataset used, 1597, was just large enough to be representative, while that for the slag particles, 3598 particles, was comfortably large enough to be representative of its class. These two particle kinds were very similar in their aspect ratios (see Table 1).

In all the VRML particle images above, the general qualitative observation was made that the virtual particles seemed to have more "lobes" than do the real particles, even though statistically, for the parameters studied, there is very good agreement between real and virtual particles. One way to capture this apparent difference quantitatively is through looking at the mean curvatures of the particles. The mean curvature of a surface at a point is the sum of the inverses of the principal radii of curvature at that point [4], normalized so that the mean curvature of a sphere, which is the same at every point, is equal to the (positive) inverse of the sphere radius. The standard deviation of the mean curvature integrated over a particle surface can also be defined using the average of the squared mean curvature and the square of the average mean curvature, both averaged over a particle surface. For a sphere, the standard deviation of the mean curvature over the surface is zero. For a general particle, the curvature will vary over the surface and so the standard deviation of the mean curvature will be non-zero.

It is first instructive to see, for a single particle, how the mean curvature and its standard deviation vary with the number of spherical harmonic coefficients used to define its surface. Figure 16 shows both quantities plotted vs. N, the maximum value of n used to define the surface of a single Wilson A particle. The mean curvature does not appear to vary much at all from the N=0 value. For N=0, the particle is a sphere. This seems to be true for all particles examined, both real and virtual. However, the standard deviation of the mean curvature starts out at zero, which is true for a sphere, then appears to increase monotonically with N. A particle with equal

volume but with more lobes can have the almost the same integrated mean curvature as a sphere, since more positive values can cancel out more negative regions, but the standard deviation of the mean curvature should increase as higher values of N are used to represent a given particle. One should remember that all the particle types considered in this paper were all star-shaped and mineral-based – the previous statement might not apply to more "exotic" particles.

However, the distribution of the integrated mean curvature and the standard deviation of the mean curvature for the entire Wilson A particle set, real and virtual, are almost identical between the real and virtual particles, so are not shown here. The very small differences can be accounted for by the fact that the average value of N used for the real Wilson A particles was about 22, with a maximum value of 26, while N=24 was used for every virtual particle, since the virtual particles had accurate particle representations, in terms of the Gaussian curvature criterion [4], up to N = 24 (see Fig. 16). This small difference in the average maximum value of n used between the real and virtual particles may explain some of the shape differences seen in the VRML images, though perhaps not all. Any unexplained qualitative differences between the images of the real and virtual particles would have to be explained by some more subtle correlation between the SH coefficients as n increases, which is being missed or not addressed with sufficient accuracy in the current virtual particle generation process.

5. Conclusions

The work on generating virtual particles based on a real particle dataset has been extended in the following ways.

- Since the particle size distribution of the real particle data set is arbitrary, the numerical technique can now handle this randomness directly, rather than trying to fit this distribution with gamma functions. This greatly improves the shape parameter agreement between the real and virtual particles, for any size real particle dataset. The higher-order coefficients appear to have a much smoother distribution and so can be readily fit with simple distributions like gamma and beta functions. All quantitative shape parameters agree very closely between real and virtual particles, which will allow the virtual particles to be used in models that require large numbers of particles.
- The virtual particle generation algorithm has been converted from a MATLAB code into a parallel Fortran 90 code, so that the run time for generating 10 000 virtual particles from a similar size real particle database has been reduced from weeks to less than one hour of processing time. Computing the geometrical properties of the virtual particles also uses a parallel algorithm, and only takes a few hours on approximately 100 processors. Much larger real particle datasets of many different kinds can now be used to generate virtual particles - certainly up to 100 000 real and virtual particles are readily handled in run times of a few hours – so that now a very fast method is available for generating an unlimited number of virtual particles based on a real particle dataset. This should be useful to any kind of model generation (e.g. packing algorithms, discrete element models).
- The dependence of the average values of various shape/size parameters (e.g. L and VESD) on the size of the real particle dataset can be used to indirectly decide whether or not enough real particles have been employed so that they are representative of their particle class. On the order of 10 000 (at least) real Wilson A particles are needed to be

used to ensure this, and 5000 Wilson B particles. Only about 1000 real particles were needed for the CC and slag particles, and only about 500 C109 sand particles. This difference in number did not appear to be strongly correlated with the size of the L/T and W/T ratios, although the C109 sand particles did have both the smallest values of the ratios and the number of real particles needed to be representative.

- When comparing 3D VRML visualizations of the virtual particles, they seem to be a bit too "lumpy", i.e. have more lobes than do the real particles. This was not explained by any differences in integrated mean curvature or the standard deviation of mean curvature, which generated almost the same distribution for the real and the virtual Wilson A particles. A small difference in the maximum value of n used might explain part of this difference. Future work will be to further define this effect mathematically and then fine-tune the virtual particle generation method to build-in this effect so that the virtual particles become even more similar, in a visual sense, to the real particles.

6. Acknowledgements

We would like to thank OMYA, Granite Rock (and especially Michael Taylor), U.S. Silica, and Aggregate Industries for supplying materials, and Brookhaven National Laboratory for supplying time on its X-ray CT beamline.

7. References

[1] J.F. Douglas and E.J. Garboczi, "Intrinsic viscosity and polarizability of particles having a wide range of shapes," Advances in Chemical Physics **91**, 85-153 (1995).

[2] M.L. Mansfield, J.F. Douglas, and E.J. Garboczi, Intrinsic viscosity and the electrical polarizability of arbitrarily shaped objects, Phys. Rev. E **64**, 61401-61416 (2001).

[3] D.W. Luerkens, Theory and Application of Morphological Analysis: Fine Particles and Surfaces, CRC Press, Boca Raton, FL, 1991.

[4] E.J. Garboczi, Three-dimensional mathematical analysis of particle shape using x-ray tomography and spherical harmonics: Application to aggregates used in concrete, Cem. Conc. Res. **32**, 1621-1638 (2002).

[5] M.A. Taylor, E.J. Garboczi, S.T. Erdogan, and D.W. Fowler, Some properties of irregular particles in 3D, Powder Technology **162**, 1-15 (2006).

[6] S.T. Erdogan, P.N. Quiroga, D.W. Fowler, H.A. Saleh, R.A. Livingston, E.J. Garboczi, P.M. Ketcham, J.G. Hagedorn, and S.G. Satterfield, Three-dimensional shape analysis of coarse aggregates: New techniques for and preliminary results on several different coarse aggregates and reference rocks, Cement and Concrete Research 36, 1619-1627 (2006).

[7] S.T. Erdogan, D.W. Fowler, and E.J. Garboczi, Shape and size of microfine aggregates: X-ray microcomputed tomography vs. laser diffraction, Powder Technology 177 (2): 53-63 (2007).

[8] S.T Erdoğan, X. Nie, P.E. Stutzman, and E.J. Garboczi, Micrometer-scale 3D imaging of eight cements: Particle shape, cement chemistry, and the effect of particle shape on laser diffraction size analysis. Cement and Concrete Research 40, 731–739 (2010).

[9] Enad Mahmoud, Leslie Gates, Eyad Masad, and Edward Garboczi, Comprehensive Evaluation of AIMS Texture, Angularity, and Dimensions Measurements, J. Materials Civil Eng. (2009) http://dx.doi.org/10.1061/(ASCE)MT.1943-5533.0000033

[10] E.J. Garboczi and J.W. Bullard, Shape analysis of a reference cement, Cem. Conc. Res. 34, 1933-1937 (2004).

[11] G.S. Cheok, W.C. Stone, and E.J. Garboczi, Using LADAR to characterize the 3D shape of aggregates: Preliminary results, Cement and Concrete Research **36**, 1072-1075 (2006).

[12] Lorenz Holzer, Robert Flatt, S.T. Erdogan, X. Nie, E.J. Garboczi, Shape comparison of a cement between nano-focused-ion-beam and X-ray microcomputed tomography, J. Amer. Ceram. Soc. in press (2010).

[13] M. Grigoriu, E.J. Garboczi, and C. Kafali, Spherical harmonic-based random fields for aggregates used in concrete, Powder Technology 166, 123-138 (2006).

[14] G. Arfken, Mathematical Methods for Physicists 2nd Ed., Academic, New York, 1970.

[15] E.J. Garboczi, Three Dimensional Shape Analysis of JSC-1A Simulated Lunar Regolith Particles, to be published in Powder Tech. (2011).

[16] E.J. Garboczi, X. Liu, and M.A. Taylor, The Shape of a Blasted and Crushed Rock Material over More than Three Orders of Magnitude: 20 μm to 60 mm, in preparation for Powder Technology (2010).

[17] “Ottawa sand” is sand that comes from the historic deposits located at Ottawa, Illinois, which have been mined for well over 100 years.

[18] S.T. Erdoğan, A. Forster, G. Lespinasse, P.E. Stutzman, and E.J. Garboczi, Characterization of Ottawa sand: Optical and scanning electron microscopy, X-ray tomography, X-ray diffraction, and instrumented nanoindentation, to be submitted to Cement and Concrete Composites (2010).

Table 1: Description of materials used in this study

Material	Type	Application	Upper size limit	# of particles acquired	<L/T>	<W/T>
Wilson A	Crushed grano-diorite, composed of feldspar and hornblende	Concrete, asphalt, base stone	< 700 μm	15 829	2.065	1.516
C109	Naturally rounded silica sand	Standard portland cement mortars	< 700 μm	2202	1.781	1.404
Slag	Ground granulated blast furnace slag	Cement substitute in concrete	< 70 μm	3598	2.030	1.529
CC	Ground calcium carbonate	Industrial filler	< 70 μm	1597	2.153	1.583
Wilson B	Crushed grano-diorite, composed of feldspar and hornblende	Concrete, asphalt, base stone	< 300 μm	22 556	2.278	1.582

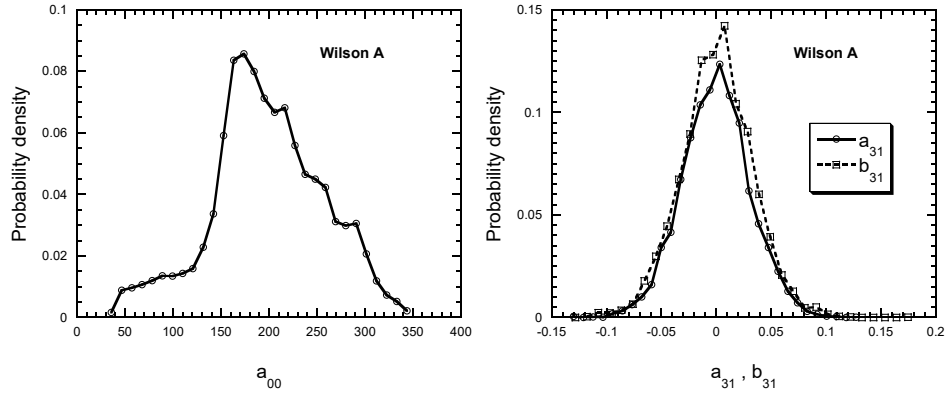

Figure 1: (a) The differential size distribution, as measured by A_{00}, of the actual 15 829 Wilson A particles; (b) the probability density of the values of the SH coefficients a_{31} and b_{31}.

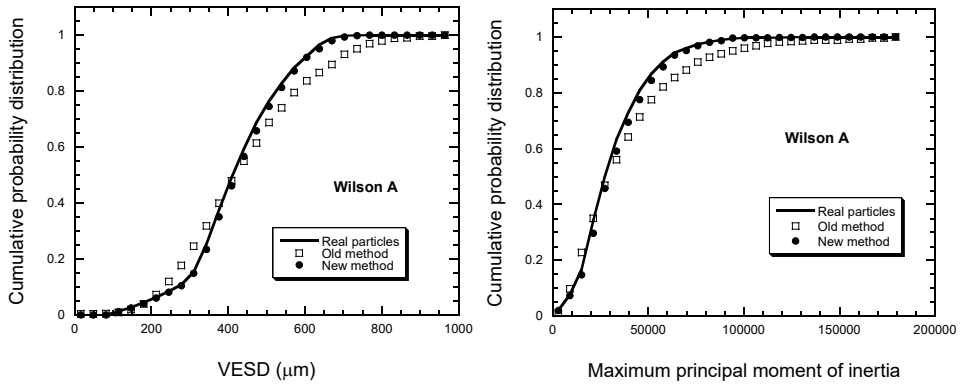

Figure 2: (a) cumulative probability distribution for VESD for the Wilson A particles, comparing the curves for the real particles and for the virtual particles using both the old and new numerical methods; (b) cumulative probability distribution for the maximum principal moment of inertia for the Wilson A particles, comparing the curves for the real particles and for the virtual particles using both the old and new numerical methods.

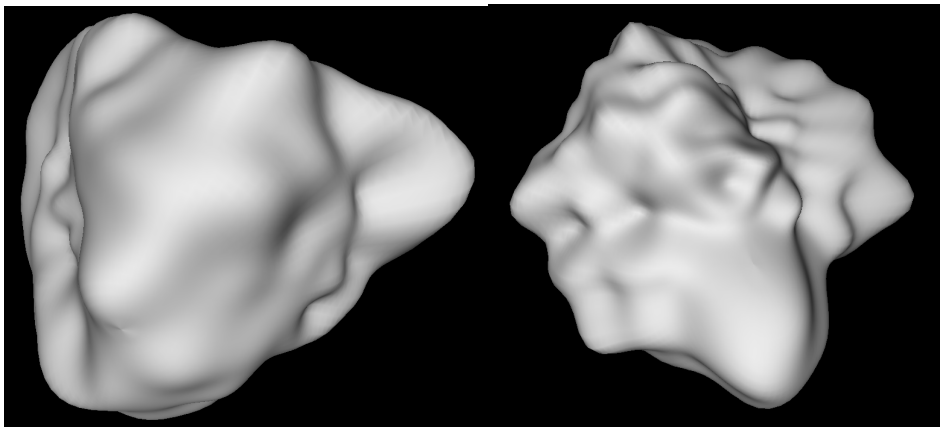

Figure 3: Wilson A VRML (left, real) (right, virtual)

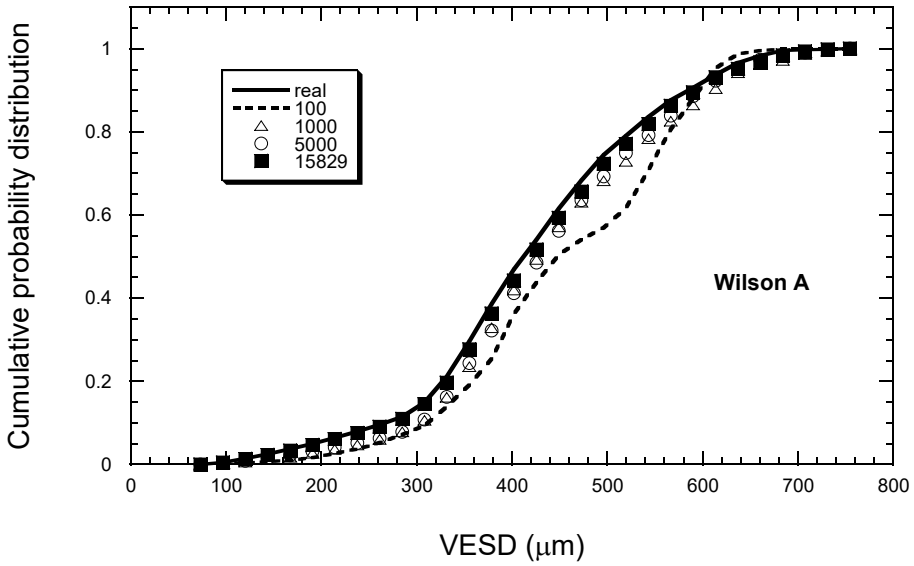

Figure 4: Cumulative probability distribution (volume basis) for the VESD of the Wilson A particles – real particle and virtual (improved method) particle results where the virtual particle results were based on the statistics of different numbers of real Wilson A particles.

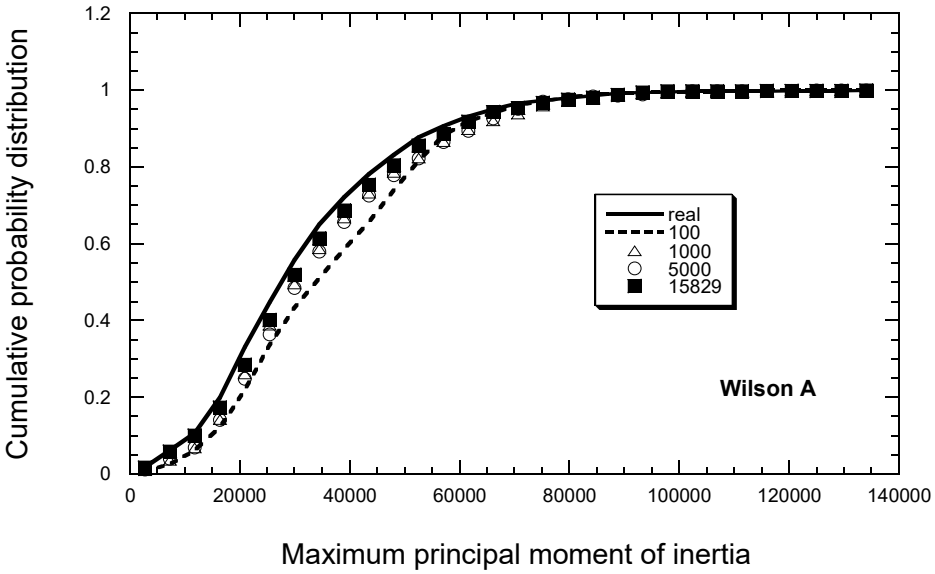

Figure 5: Cumulative probability distribution (volume basis) for the maximum principal moment of inertia of the Wilson A particles – real particle and virtual (improved method) particle results where the virtual particle results were based on the statistics of different numbers of real Wilson A particles.

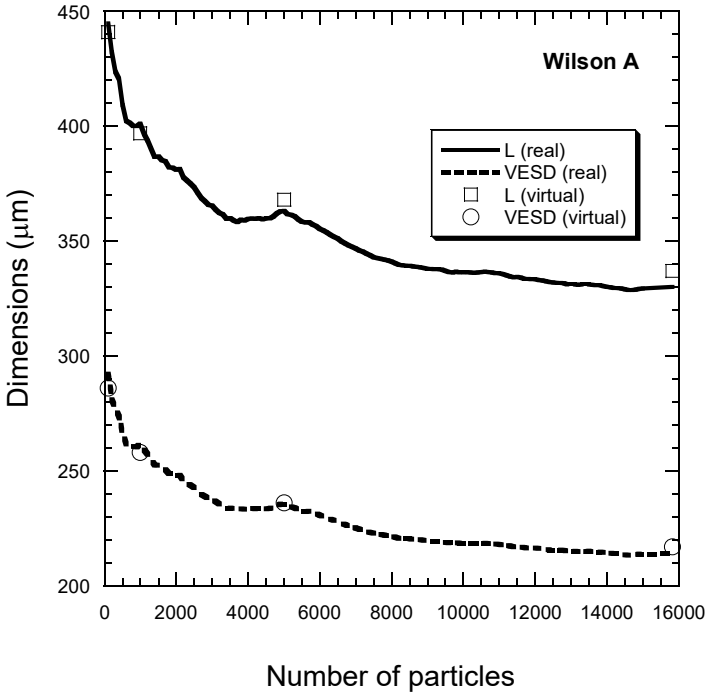

Figure 6: The average values of L and VESD for the Wilson A particles, plotted vs. the number of real particles that were averaged over to determine these values (curves). The points were from averages over 10 000 virtual particles, generated using the given number of real particles.

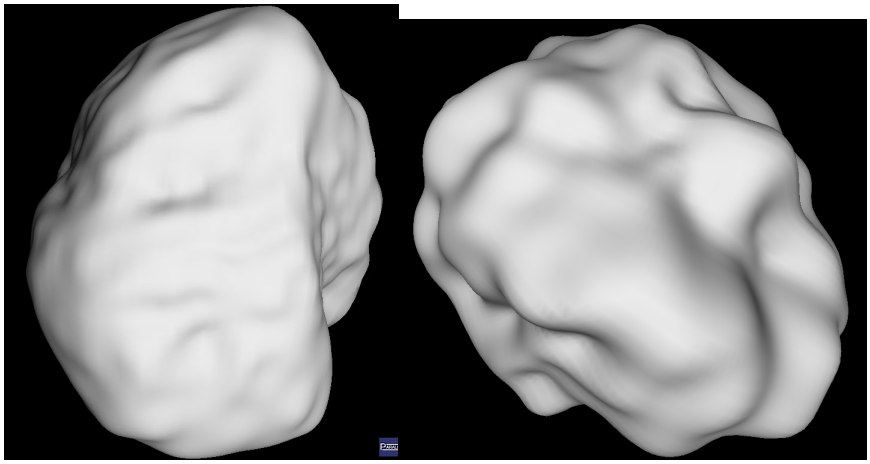

Figure 7: C109 VRML images (left, real) (right, virtual)

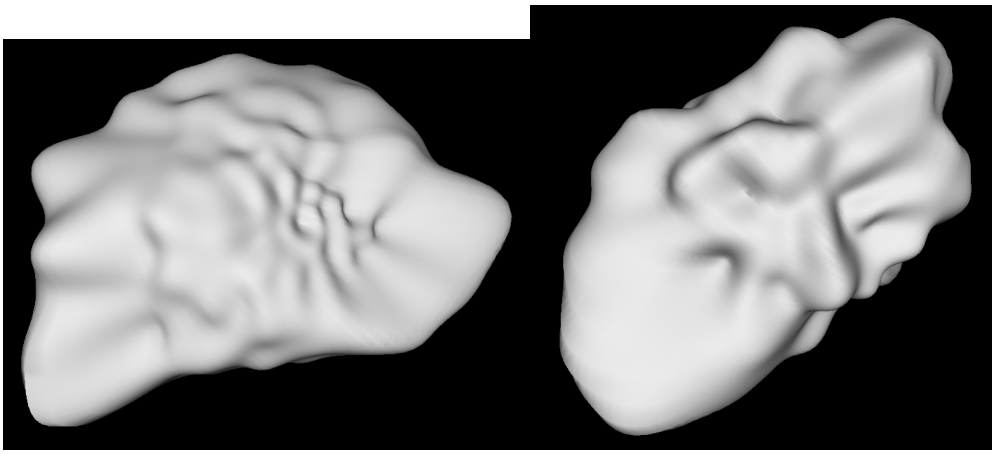

Figure 8: Wilson B VRML images (left, real) (right,virtual)

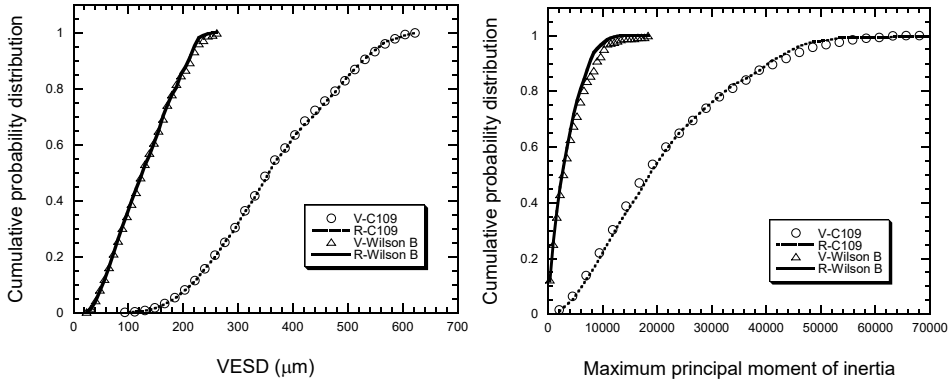

Figure 9: Left – VESD cumulative probability distribution for C109 sand and Wilson B particles, right – maximum principal moment of inertia cumulative probability distribution for C109 sand and Wilson B particles.

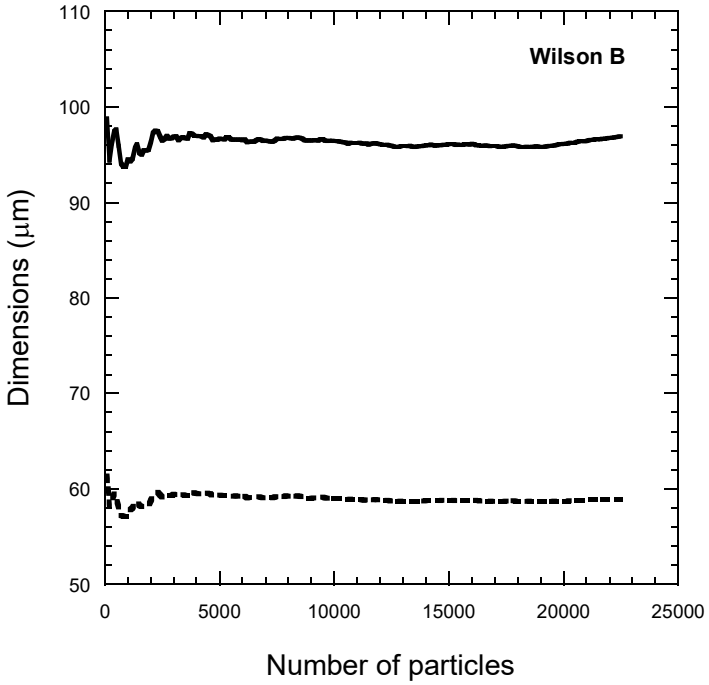

Figure 10: The average values of L and VESD for the Wilson B particles, plotted vs. the number of real particles that were averaged over to determine these values.

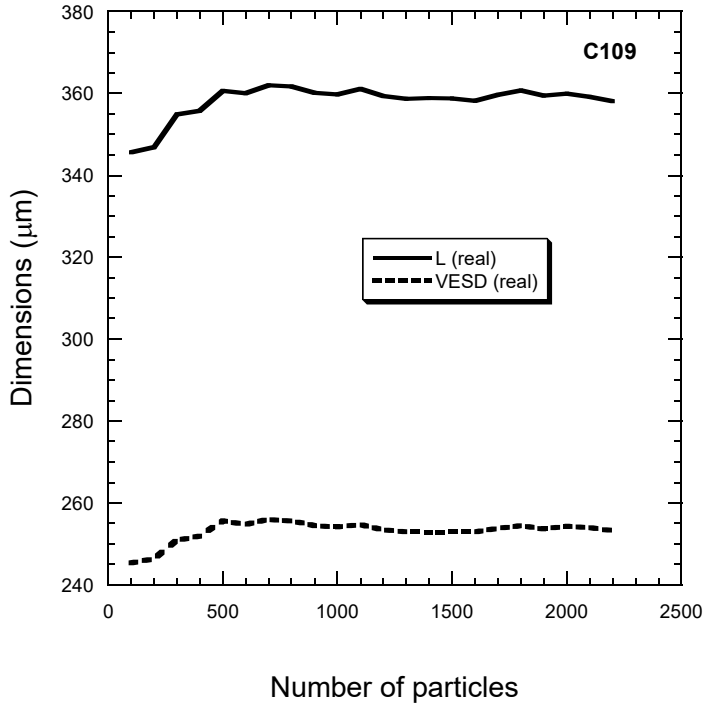

Figure 11: The average values of L and VESD for the C109 particles, plotted vs. the number of real particles that were averaged over to determine these values.

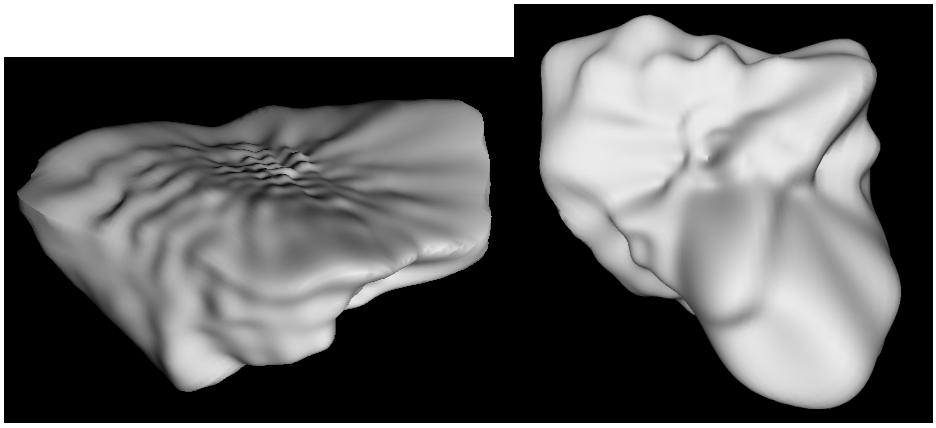

Figure 12: Slag VRML images (left, real) and (right, virtual)

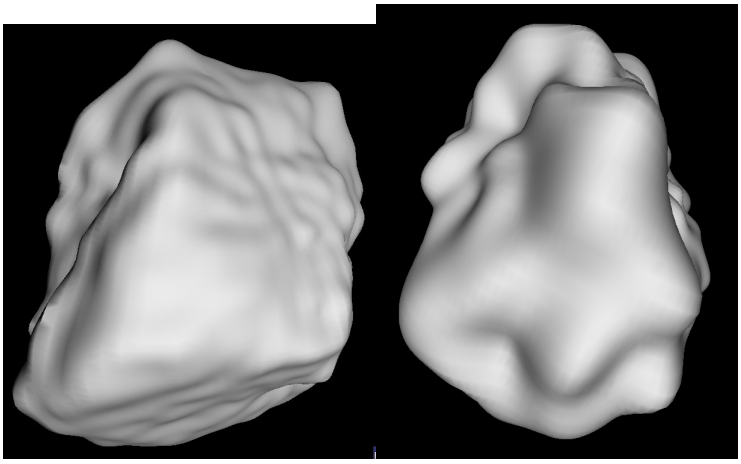

Figure 13: CC VRML images (left, real) (right, virtual)

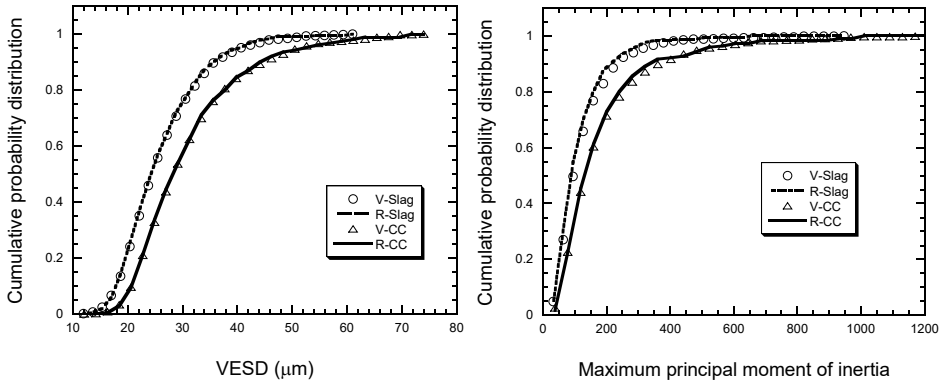

Figure 14: Left – VESD cumulative probability distribution for slag and calcium carbonate (CC) particles , right – maximum principal moment of inertia cumulative probability distribution for slag and calcium carbonate (CC) particles.

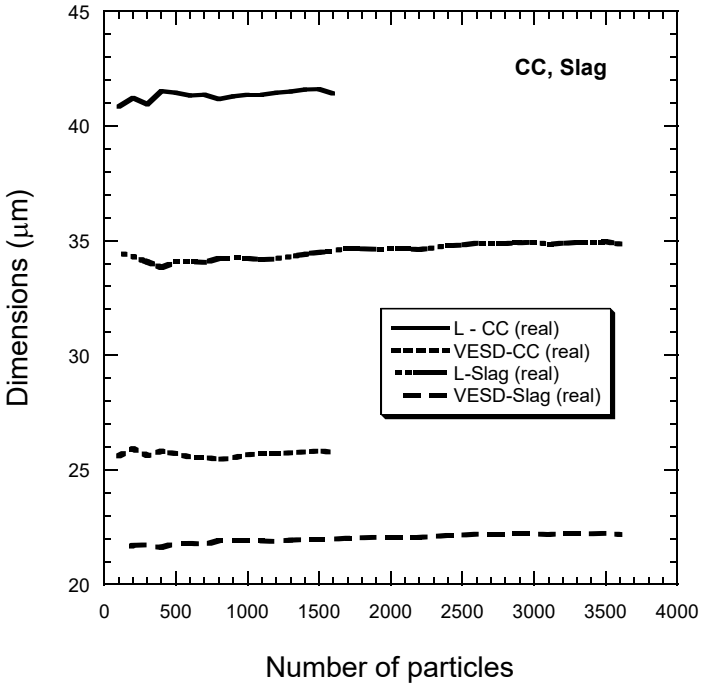

Figure 15: The average values of L and VESD for the CC and slag particles, plotted vs. the number of real particles that were averaged over to determine these values.

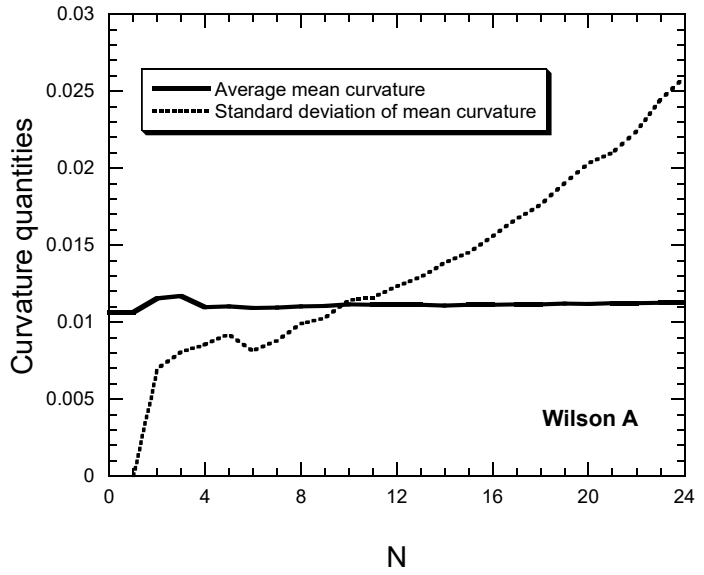

Figure 16: The integrated mean curvature and the standard deviation of the mean curvature as a function of N, the maximum value of the spherical harmonic coefficient n used to represent the particle, for a single Wilson A particle. The dimension of the curvature quantities are reciprocal length.